Reduced structural connectivity within a prefrontal-motor-subcortical network in amyotrophic lateral sclerosis

Reduced structural connectivity within a prefrontal-motor-subcortical network in amyotrophic lateral sclerosis

Abstract

Purpose: To investigate white matter structural connectivity changes associated with amyotrophic lateral sclerosis (ALS) using network analysis and compare the results with those obtained using standard voxel-based methods, specifically Tract-based Spatial Statistics (TBSS).

Materials and methods: MRI data were acquired from 30 patients with ALS and 30 age-matched healthy controls. For each subject, 85 grey matter regions (network nodes) were identified from high resolution structural MRI, and network connections formed from the white matter tracts generated by diffusion MRI and probabilistic tractography. Whole-brain networks were constructed using strong constraints on anatomical plausibility and a weighting reflecting tract-averaged fractional anisotropy (FA).

Results: Analysis using Network-based Statistics (NBS), without *a priori* selected regions, identified an impaired motor-frontal-subcortical subnetwork (10 nodes and 12 bidirectional connections), consistent with upper motor neuron pathology, in the ALS group compared with the controls (p = 0.020). Reduced FA in three of the impaired network connections, which involved fibres of the corticospinal tract, correlated with rate of disease progression ($p \leq$ 0.024). A novel network-tract comparison revealed that the connections involved in the affected network had a strong correspondence (mean overlap of 86.2%) with white matter tracts identified as having reduced FA compared with the control group using TBSS.

Conclusion: These findings suggest that white matter degeneration in ALS is strongly linked to the motor cortex, and that impaired structural networks identified using NBS have a strong correspondence to affected white matter tracts identified using more conventional voxel-based methods.

Key Words: amyotrophic lateral sclerosis, white matter, tractography, brain networks, connectome

Amyotrophic lateral sclerosis (ALS), the most common form of motor neuron disease, is a devastating adult-onset neurodegenerative disorder (1). The disease is characterized by chronic and usually rapid degeneration of the upper motor neurons of the motor cortex, and the lower motor neurons of the brain stem and spinal cord. Approximately 5–15% of sufferers are also afflicted with frontotemporal dementia (2), and a proportion of non-demented patients present with specific cognitive impairment suggesting that the disease also affects extra-motor regions (3). Though the etiology of ALS is not well understood, MRI has proved useful in probing associated white matter degeneration. Previous studies using diffusion MRI (dMRI) have identified reduced white matter integrity in corticospinal tract (4-14), corpus callosum (9,12,14) and uncinate fasciculus (10,12,14). Functional MRI studies have also identified abnormalities in extra-motor brain areas, including prefrontal regions (16,17), while voxel-based morphometry analyses have found evidence of reduced grey matter volumes in the superior, medial and mid frontal gyri, and anterior cingulate (18,19), and reduced white matter volume and integrity in frontotemporal regions (19,20). Such findings have lead to the suggestion that ALS may be a progressive multi-system disorder (21-23).

However, many of these studies have relied on region-specific analyses, which are typically constrained to a limited number of major white matter pathways or cortical areas. It is possible that whole-brain network analysis of structural connectivity between brain regions (24), involving many hundreds of potential connections, may help identify more widespread reductions in connectivity associated with ALS. Structural networks can be constructed from MRI data, with network nodes identified from high-resolution structural MRI, and network connections formed by white matter tracts generated from dMRI and tractography. Network measures derived from graph-theory can then be used to characterize patterns of connectivity in individuals or across populations (25). Alternatively, statistical methods, such as Network-based Statistics (NBS) (26), can be used to identify differences in connectivity in case-control studies. The utility of NBS has previously been demonstrated in schizophrenia (26,27) and ALS (28,29), although how the results compare to other brain-wide MRI analysis techniques remains to be determined.

In this study, we investigate whether whole-brain structural network analysis, without *a priori* selected regions, can provide further insights into global white mater changes associated with ALS, and whether there is any association between the resulting network measures and disease severity and rate of progression. Finally, since structural network analysis is a relatively novel approach for characterizing white matter abnormalities in disease, we also investigate whether there is correspondence between affected networks and reduced integrity in white matter tracts identified using more standard brain-wide voxel-based methods.

MATERIALS AND METHODS

Participants

Thirty patients and 30 age-matched healthy controls were recruited and underwent MRI scanning between July 2009 and April 2012 as part of a wider study examining relationships between cognitive function and brain structure in ALS (10). The patient and control subjects have previously been described in Bastin et al. (6) and Pettit et al. (10). The patient group was recruited from regional ALS services at the following sites throughout Scotland: Western General Hospital, Edinburgh; Southern General Hospital, Glasgow; Ninewells Hospital, Dundee; and from the Motor Neuron Disease register for Scotland, University of Edinburgh. All had clinical and electrophysiological evidence of combined upper and lower motor neuron involvement and fulfilled the revised El Escorial criteria for clinical definite and probable ALS (30). Exclusion criteria included the presence of another neurological disorder, presence or history of psychiatric disorder, and the presence of severe cardiovascular risk factors. Disease severity was assessed using the ALS Functional Rating Scale-Revised (ALSFRS-R) (31), while the rate of disease progression was determined using the following equation (13,32):

$$\text{Disease progression rate} = (48 - \text{ALSFRS-R score})/\text{disease duration}. \quad (1)$$

The control group was recruited from the University of Edinburgh Psychology Department's Volunteer Participant Panel, or from spouses, friends or relatives of patients. The study was approved by the Scottish local (LREC 08/S11ADMIN/67), multicentre (MREC 08/MRE00/50) and Department of Psychology, University of Edinburgh Research Ethics Committees. All subjects gave written informed consent.

MRI Acquisition

All imaging data were acquired using a GE Signa Horizon HDxt 1.5 T clinical scanner (General Electric, Milwaukee, WI, USA) equipped with self-shielding gradient set (33 mT m^{-1} maximum gradient strength) and manufacturer supplied 8-channel phased-array head coil. For the dMRI protocol, ungated single-shot spin-echo echo-planar (EP) diffusion-weighted whole-brain volumes (b = 1000 s mm^{-2}) were acquired in 64 non-collinear directions, along with seven T_2-weighted volumes (b = 0 s mm^{-2}) (33). The repetition and echo times were 16.5 s and 98.3 ms respectively. Seventy-two contiguous axial 2 mm thick slices were acquired resulting in 2 mm isotropic voxels. In the same session, high resolution 3D T_1-weighted inversion-recovery-prepared fast spoiled gradient-echo (FSPGR) volumes were acquired in the coronal plane with 180 contiguous 1.3 mm thick slices resulting in voxel dimensions of 1 × 1 × 1.3 mm.

Image Processing

An automated connectivity mapping pipeline was used to construct white matter structural networks from the T_1-weighted and dMRI data. This framework is described below with settings informed by findings from a test-retest study using healthy volunteers of comparable age (34).

Each T_1-weighted FSPGR volume was first divided into distinct neuroanatomical regions using the volumetric segmentation and cortical reconstruction performed with the FreeSurfer image analysis suite using the default parameters (http://surfer.nmr.mgh.harvard.edu). The Desikan-Killiany atlas delineated 34 cortical structures per hemisphere (35,36). Additionally, subcortical segmentation was applied to obtain the brain stem and eight further grey matter structures per hemisphere: accumbens area, amygdala, caudate, hippocampus, pallidum, putamen, thalamus and ventral diencapahlon (37,38). As a result, 85 regions-of-interest (ROI) were retained per subject. The results of the segmentation procedure were used to construct grey and white matter masks for each subject. Using the FDT package in FSL (http://fsl.fmrib.ox.ac.uk/fsl), the dMRI data underwent eddy current correction to reduce systematic imaging distortions and bulk patient motion artifacts using affine registration to the first T_2-weighted EP volume of each subject (39). Fractional anisotropy (FA) was calculated at each voxel location to indicate the degree of anisotropic water molecule diffusion (40). Skull stripping and brain extraction were performed on the T_2-weighted EP volumes and applied to the FA volume of each subject (41). A cross-modal nonlinear registration method was then used to align neuroanatomical ROI from T_1-weighted volume to diffusion space. As a first step, linear registration was used to initialize the alignment of each brain-extracted FA volume to the corresponding FreeSurfer extracted T_1-weighted brain using a mutual information cost function and an affine transform with 12 degrees of freedom (39). Following this initialization, a nonlinear deformation field based method was used to refine local alignment. FreeSurfer segmentations and anatomical labels were then aligned to diffusion space using nearest neighbor interpolation (42). For each subject, a binary mask was formed in diffusion space from all grey and white matter voxels obtained from FreeSurfer. These masks were then used to constrain the tractography output.

Tractography

Whole-brain tractography was performed using an established probabilistic algorithm (FDT BedpostX/ProbtrackX; http://fsl.fmrib.ox.ac.uk/fsl) (43,44). Probability density functions, which describe the uncertainty in the principal directions of diffusion, were computed with a two-fiber model per voxel (44). Streamlines were then constructed by sampling from these

distributions during tracking using 100 Markov Chain Monte Carlo iterations with a fixed step size of 0.5 mm between successive points. Tracking was initiated from all white matter voxels and streamlines were constructed in two collinear directions until terminated by the following stopping criteria designed to minimize the amount of anatomically implausible streamlines: (i) exceeding a curvature threshold of 70 degrees; (ii) entering a voxel with FA below 0.1 (28); (iii) entering an extra-cerebral voxel; (iv) exceeding 200 mm in length; and (v) exceeding a *distance ratio metric* of 10. The distance ratio metric excludes implausibly tortuous streamlines (45). For instance, a streamline with a total path length ten times longer than the distance between end points was considered to be invalid. The values of the curvature, anisotropy and distance ratio metric constraints were set empirically and informed by visual assessment of the resulting streamlines.

Network Construction

Networks were constructed by recording connections between all ROI pairs (network nodes). The endpoint of a streamline was considered to be the first grey matter ROI encountered when tracking from the seed location. A *streamline density* weighting, a_{ij}, recording the interconnecting streamline density corrected for ROI size was computed:

$$a_{ij} = \frac{2}{g_i + g_j}|S_{ij}|, \tag{2}$$

where $|S_{ij}|$ is the count of the set of all streamlines found between nodes i and j (and $S_{ij} = S_{ji}$), and g_i and g_j the number of grey matter voxels in nodes i and j. The rationale for the normalization by g is to correct for between-subject variability in grey matter volume, since the number of possible entry/exit points per region is proportional to the grey matter volume (46). As tractography is prone to producing false connections (47), we used prior knowledge of white matter anatomy to discard a proportion of spurious connections. Any implausible streamlines traversing from one cortical hemisphere to any contralateral subcortical node were discarded (48). To reduce spurious connections, a two-step threshold on the network weights was then applied: (i) for each subject, discard the weakest 25% of weights in the matrix by connection probability (Eq. 2); (ii) across the cohort, only retain connections which occur in at least 50% of subjects. The second step is required to discard connections which have been removed for some subjects, but not others, by the first step. From the remaining set of streamlines, *FA-weighted* networks were then computed by recording the mean FA value along interconnecting streamlines:

$$a_{ij} = \frac{1}{|S_{ij}|} \sum_{s \in S_{ij}} \frac{\sum_{v \in V_s} \mathrm{FA}(v)}{m_s}, \quad (3)$$

where V_s is the set of voxels (of size m_s) found along the streamline s between nodes i and j, and FA measures the diffusion anisotropy per voxel. If no streamlines were found between a pair of nodes, the corresponding matrix entry was set to zero. Self-connections were removed. For each FA-weighted matrix, three global network measures were then computed (25), namely, the *network strength* (the average sum of weights per node), *network clustering coefficient* (an average measure of local connectivity) and the *network efficiency* (the average of the inverse shortest path length).

Statistical Analysis

The global network properties, and measures of disease severity and rate of progression were assessed for normality using the Shapiro-Wilk test with non-normality accepted at the $p < 0.05$ level of significance. Group contrasts were performed using a two-sample *t*-test for Normally distributed data. The two-tailed probability level was used for all global comparisons. Correlations for non-normal variables were computed with Spearman's rank correlation coefficient (ρ).

Network Analysis

Firstly, in order to assess any differences in global connectivity between the patient and control groups, the global network measures were tested with uncorrected $p < 0.05$ being considered statistically significant. Secondly, network connections were compared between the patient and control groups using NBS (https://sites.google.com/site/bctnet/comparison/nbs) (26), without *a priori* selected regions. For 85 node networks there are 3570 possible network connections. As a result, standard statistical tests may be under-powered when corrected for multiple comparisons. NBS is an alternative approach which exploits the extent to which the connections identified by the contrast are interconnected to offer a potential gain in statistical power, for which the significance of maximally connected subnetworks are assessed rather than individual connections (26). In the NBS framework, first a two-sample one-tailed *t*-test was performed at each of the 3570 network connections in order to identify reduced white matter integrity in the patient group compared with the controls. Secondly, a set of suprathreshold edges and the corresponding set of maximally connected network components was computed by a network-defining threshold on the *t*-statistics. Permutation testing, which randomly exchanged the group to which each subject belonged, was used over 5000 iterations to estimate the distribution of component size and compute a corrected *p*-value for the

maximally connected subnetwork(s). In NBS terminology, the 'intensity' of each maximally connected network was tested rather than the 'extent' (size of the network) as this directly assesses the magnitude of the test statistic. For completeness, we also repeated the NBS analysis to identify any increases in FA between patient and control groups. In addition, the streamlines involved in any network identified by NBS were used to compute maps of streamline density per voxel for each subject (49). As discussed below, the cerebral areas identified in these maps were then compared with the findings from a voxel-based analysis of white matter differences between patient and control groups.

Tract-based Spatial Statistics

Voxel-based analysis of group differences in FA was provided by Tract-based Spatial Statistics (TBSS; http://fsl.fmrib.ox.ac.uk/fsl) (50). Firstly, a nonlinear deformation was used to align the FA map of each subject to a white matter template in standard space. White matter masks were 'skeletonised' (morphologically thinned) in order to obtain the centre-line of the principle white matter pathways, while minimizing the impact of registration error and partial volume effects. Voxel-wise FA was then compared between groups within the white matter skeleton. Finally, permutation testing assigned a corrected *p*-value to each voxel, for which $p < 0.05$ was considered significant. Comparisons were performed to identify both reduced and increased FA in the patient group compared with the controls.

Comparison Between Network and Voxel-based Analyses

To provide a measure of the agreement between network and voxel-based analyses, we measured the overlap between the impaired connections identified by NBS and the white matter contrast maps produced by TBSS. Firstly, the TBSS corrected *p*-value contrast maps were thresholded at $p < 0.05$. These masks were then transformed to each subject's native space using the nonlinear transforms computed by TBSS. For each subject, a measure of overlap per connection based on streamline density was computed:

$$r_{ij} = \frac{|D_{ij}|}{|S_{ij}|}, \tag{4}$$

where $|S_{ij}|$ is the count of all streamlines found between nodes i and j, and $|D_{ij}|$ is the count of streamlines which pass through at least one voxel of the TBSS corrected *p*-value contrast map (where $D_{ij} \subset S_{ij}$). For each network connection, this metric produces a score between 0 and 1, reflecting the proportion of streamlines between nodes i and j which pass through any voxel

identified by TBSS. A *t*-test was used to compare the mean overlap for connections within the observed network against the non-zero connections outwith this network.

RESULTS

Participants

Of the 30 patients, 26 had sporadic ALS and four had a history of suspected ALS in a first-degree relative. Ten patients had bulbar onset, 11 had upper limb onset and nine had lower limb onset. Four patients met criteria for ALS with cognitive impairment and one fulfilled criteria for possible behavioral variant frontotemporal dementia. The mean age of the patients (17 male) was 58.3 ± 11.2 years (mean ± standard deviation). The mean age of the 30 control subjects (16 male) was 58.5 ± 12.0 years. There were no significant differences between groups in either age or gender. For the patient group, the mean ALFRS-R score was 38.8 ± 6.76, the mean disease duration was 24.0 ± 18.3 months and the corresponding disease progression rate was 0.49 ± 0.4 units month^{-1}. Two patients had to be excluded from this study due to incomplete MRI data or excessive motion artifact.

Network Analysis

Figure 1 shows an example of segmentation and tractography for one representative healthy control. Visual inspection of the segmentations for each subject indicated that the FreeSurfer procedure provided plausible brain extraction, tissue segmentation and cortical labeling (Figure 1a). Approximately 6 million streamlines were seeded per subject (Figure 1b). Visual assessment of the streamlines remaining following network thresholding indicated that the majority of streamlines were anatomically plausible. Figure 1(c) shows the mean connectivity matrix averaged across all subjects. Figure 1(d) displays the histograms of network weights in patients and controls, and indicates that there is very little variation in global connectivity between the two groups. All global network measures were found to be approximately normally distributed. Although all global measures were lower in the ALS group compared with the controls, individual *t*-tests indicated that these differences were not significant (Table 1). However, as displayed in Figure 2, NBS identified a subnetwork (10 nodes and 12 bidirectional connections) of impaired connectivity in the ALS group ($t = 2.6$, $p = 0.020$, corrected). This network involves four nodes within the primary motor cortex (bilateral precentral and paracentral), left superior frontal, the left-posterior cingulate and four subcortical areas (bilateral pallidum, left thalamus, left caudate). All 12 network connections are directly linked to nodes within the primary motor cortex. Table 2 shows the mean FA values in both patient and control groups, and the corresponding *t*-statistic for each of these

network connections. Overall, the connections in the affected network showed a mean reduction of 0.04 ± 0.03 (approximately 10%) in FA in the patient group compared with the controls. (The additional NBS contrast testing for increased white matter integrity in the patient group compared with the controls produced no significant results.)

Impaired Connectivity Correlates of Disease Severity and Progression Rate

Relationships between the 12 affected network connections, which showed significant differences between patient and control groups (Figure 2), and disease severity and progression rate were investigated. After false discovery rate (FDR) correction, three of the impaired network connections correlated with disease progression rate (Figure 3): left-pallidum to left-precentral (ρ = -0.52, p = 0.024); right-pallidum to right-precentral (ρ = -0.55, p = 0.017); and left-thalamus to left-precentral (ρ = -0.58, p = 0.017).

Comparison Between Network and Voxel-based Analyses

Figure 4(a) shows the areas involved in the affected network across all subjects in Montréal Neurological Institute (MNI) standard space, in terms of the mean streamline density per voxel (49).

TBSS found significant reductions in FA within the corticospinal tract and portions of the corpus callosum in patients compared with controls (Figure 4b). (TBSS found no areas of increased FA in patients compared with controls.) These regions of reduced FA identified by TBSS were found to overlap with regions involved in the affected network. Figure 5 shows the mean overlap proportion (Eq. 4) with 95% inter-percentile range for the 12 network connections identified by NBS. Notably, 11 out of 12 connections had an overlap proportion greater than 0.75, suggesting that the majority of streamlines involved in the affected network passed through white matter structures identified by TBSS as having significantly reduced FA between groups. Only the connection between left paracentral and left superior frontal gyrus had a lower score of 0.21, suggesting that the streamlines involved in this connection were in less agreement with the TBSS analysis. Overall, 73.6 ± 2.2% of the possible network connections in the patient group and 73.0 ± 2.9% in the control group had at least one streamline which passed through a region identified by TBSS as having reduced FA. Furthermore, 39.7 ± 2.3% of the network connections in the patient group and 40.1 ± 2.0% in the control group had half of the total streamlines pass through a region identified by TBSS. Crucially, however, the mean overlap proportion (Eq. 4) was 0.385 ± 0.017 for connections outside the impaired network, compared with a mean proportion of 0.862 ± 0.041 for the connections within the network. A t-test showed that these proportions were significantly different ($p << 0.001$).

DISCUSSION

This study presents a whole-brain structural network analysis of white matter connectivity changes in ALS. Global network properties indicate that the networks in both patient and control groups are similar and show a level of clustering and network efficiency comparable to other studies (28,34). Note that the absolute values of these properties are dependent on the choice of nodes and thresholding. The between-group comparison of global network properties found no brain-wide impairments in connectivity for the patient group, indicating that any impairments are localized.

Our results suggest that in the patient group, connectivity to primary motor, prefrontal, and subcortical regions is substantially reduced, in terms of tract-averaged FA, and that these impairments are predominantly localized around the motor cortex. Notably, although a brain-wide analysis was performed, without *a priori* selected regions, the network identified involved regions which are known to be associated with motor control and movement, and are consistent with upper motor neuron pathology as found in ALS. Previous dMRI studies have shown reduced white matter integrity in the corticospinal tract and corpus callosum (5,21), areas which are interlinked with several of the subcortical and motor cortex nodes within our affected network. (A quantitative tractography analysis of this cohort showed, amongst other findings, reduced FA and altered tract topology in corticospinal tract in patients compared with controls (6).) A previous ALS study identified a nine node network which comprised a comparable pattern of motor network impairment involving connections to precentral, paracentral, pallidum, frontal areas and the cingulate cortex (28). Previous functional MRI studies have identified impairments in functional connectivity associated with ALS (51). Promisingly, studies in healthy volunteers have found some convincing associations between functional and structural connectivity (46,52). However, to our knowledge, this structure-function correspondence has not yet been demonstrated in an ALS network. One recent study has produced findings which suggest that the level of functional connectedness within the motor network is correlated with the rate of disease progression (14).

Comparison between the network analysis and TBSS findings offers some insight into the correspondence between these methods. Approximately 40% of all connections had half of their total streamlines pass through a region identified by TBSS as significantly different between groups. This indicates that the abnormal white matter identified by TBSS contains a common ‘hub’ connecting grey matter regions, for instance, via portions of the corpus callosum. The comparison of the mean overlap proportion within and outwith the impaired network indicates a strong, but not perfect, agreement between the white matter identified by TBSS and the affected network identified by NBS. Notably, NBS identified one network

connection between left paracentral and left superior frontal gyrus that was unlikely to have been concluded from the TBSS analysis. Conversely, there were several connections outside the affected network which also had a high overlap proportion (close to 1), which were not identified by NBS. Due to limitations of the data, noise and tractography errors, some connections may contain spurious streamlines which cross the regions identified by TBSS.

Associations between the affected network connections and disease metrics indicate that the bilateral pallidum to precentral, and left thalamus to left precentral connections are increasingly impaired over disease progression. Notably, these affected connections involve fibers which run through the cortical to subcortical portion of the corticospinal tract. These findings provide supporting evidence for similar relationships found between disease progression and FA in the rostral corticospinal tract reported in a previous study (14). Furthermore, although some of the patients included in this study were cognitively impaired, across the whole group no meaningful correlations emerged between the affected network and measures of cognitive performance. However, the affected network did include prefrontal regional nodes (namely the superior frontal gyrus) found to be affected in our previous ROI-based analyses and related to impairments in letter fluency (10).

One strength of this study is the relatively large and well-characterized patient sample with age-matched controls. We also utilized probabilistic tractography to model multiple fiber populations in each voxel in the network analysis. Such techniques should be better able to account for branching and crossing fibers, in comparison to deterministic (diffusion tensor) tractography. In addition, previous ROI-based studies are typically limited to assessing changes in a small number of regions. However, the network analysis used in this study offers the possibility to explore ALS as a network disease, potentially involving hundreds of connections. Furthermore, in comparison to TBSS or other template-based methods, network analysis is performed in native rather than standard space, thereby accounting for individual differences in white matter structure and providing a more representative reconstruction of the underlying axonal wiring. Like previous network studies (28,29), we chose to use FA-weighted networks, rather than streamline density, as FA is likely to be a more representative measure of disruption in the underlying axonal fibers in case-control studies (34).

We note that although NBS reduces the false positive rate, tractography is known to be strongly affected by measurement noise resulting in both false positive and negative connections (53,54). Some error may reflect tractography issues in estimating the underlying axonal fibers from noisy measurements; the dMRI protocol employed an ungated EP imaging sequence which may introduce motion artifacts due to pulsatile brain motion (55). Fillard et al. (56) suggested that for medium or low signal-to-noise datasets, an appropriate prior on the

spatial smoothness of either the diffusion model or the fibers is recommended for correct modeling. This merits further investigation. Other errors may be due to ROI segmentation affecting seeding. Additionally, thresholding of networks must be performed with caution. It is problematic to ensure that an arbitrary threshold removes spurious connections while retaining genuine patterns of connectivity. We believe that the two-step thresholding procedure used in this study eliminates a proportion of implausible connections without biasing the results of a group-wise analysis. However, due to the limitations of current dMRI and tractography techniques it is not possible to eliminate all false connections.

In conclusion, this study presents a whole-brain network analysis of white matter degeneration in ALS, using strong constraints on the anatomical plausibility of tracts. The key findings are that while there are no brain-wide impairments in connectivity due to ALS, an impaired motor-frontal-subcortical network of reduced white matter FA was found in the patient group. Reduced white matter FA in three of the impaired network connections, which involved fibers of the corticospinal tract, correlated with disease progression rate showing links between brain structure and clinical measures of the disease. There was also a strong correspondence between the connections identified as being impaired in the network analysis and white matter tracts identified by conventional TBSS analysis, indicating the usefulness of both approaches in characterizing the widespread effects of ALS on brain structure.

REFERENCES

1. Rowland LP, Shneider NA. Amyotrophic lateral sclerosis. N. Eng. J. Med. 2001;344:1688–1700.

2. Geser F, Martinez-Lage M, Kwong LK, Lee VM-Y, Trojanowski JQ. Amyotrophic lateral sclerosis, frontotemporal dementia and beyond: the TDP-43 diseases. J. Neurol. 2009;256:1205–1214.

3. Goldstein LH, Abrahams S. Changes in cognition and behaviour in amyotrophic lateral sclerosis: nature of impairment and implications for assessment. Lancet Neurol. 2013;12:368-380.

4. Abe O, Yamada H, Masutani Y, Aoki S, Kunimatsu A, Yamasue H, Fukuda R, Kasai K, Hayashi N, Masumoto T, Mori H, Soma T, Ohtomo K. Amyotrophic lateral sclerosis: diffusion tensor tractography and voxel-based analysis. NMR Biomed. 2004;17:411–416.

5. Agosta F, Pagani E, Petrolini M, Caputo D, Perini M, Prelle A, Salvi F, Filippi M. Assessment of white matter tract damage in patients with amyotrophic lateral sclerosis: a diffusion tensor MR imaging tractography study. AJNR Am. J. Neuroradiol. 2010;31:1457–1461.

6. Bastin ME, Pettit LD, Bak TH, Gillingwater TH, Smith C, Abrahams S. Quantitative tractography and tract shape modeling in amyotrophic lateral sclerosis. J. Magn. Reson. Imaging 2013;38:1140–1145.

7. Blain CRV, Brunton S, Williams VC, Leemans A, Turner MR, Andersen PM, Catani M, Stanton BR, Ganesalingham J, Jones DK, Williams SC, Leigh PN, Simmons A. Differential corticospinal tract degeneration in homozygous 'D90A' SOD-1 ALS and sporadic ALS. J. Neurol. Neurosurg. Psychiatry 2011;82:843–849.

8. Ciccarelli O, Behrens TE, Altmann DR, Orrell RW, Howard RS, Johansen-Berg H, Miller DH, Matthews PM, Thompson AJ. Probabilistic diffusion tractography: a potential tool to assess the rate of disease progression in amyotrophic lateral sclerosis. Brain 2006;129:1859–1871.

9. Douaud G, Filippini N, Knight S, Talbot K, Turner MR. Integration of structural and functional magnetic resonance imaging in amyotrophic lateral sclerosis. Brain 2011;134:3470–3479.

10. Pettit LD, Bastin ME, Smith C, Bak TH, Gillingwater TH, Abrahams S. Executive deficits, not processing speed relates to abnormalities in distinct prefrontal tracts in amyotrophic lateral sclerosis. Brain 2013;136:3290–3304.

11. Sarica A, Cerasa A, Vasta R, Perrotta P, Valentino P, Mangone G, Guzzi PH, Rocca F, Nonnis M, Cannataro M, Quattrone A. Tractography in amyotrophic lateral sclerosis using a novel probabilistic tool: a study with tract-based reconstruction compared to voxel-based approach. J. Neurosci. Methods. 2014;224:79-87.

12. Sarro L, Agosta F, Canu E, Riva N, Prelle A, Copetti M, Riccitelli G, Comi G, Filippi M. Cognitive functions and white matter tract damage in amyotrophic lateral sclerosis: a diffusion tensor tractography study. AJNR Am. J. Neuroradiol. 2011;32:1866-1872.

13. van der Graaff MM, Sage CA, Caan MWA, Akkerman EM, Lavini C, Majoie CB, Nederveen AJ, Zwinderman AH, Vos F, Brugman F, van den Berg LH, de Rijk MC, van Doorn PA, Van Hecke W, Peeters RR, Robberecht W, Sunaert S, de Visser M. Upper and extra-motoneuron involvement in early motoneuron disease: a diffusion tensor imaging study. Brain 2011;134:1211–1228.

14. Verstraete E, van den Heuvel MP, Veldink JH, Blanken N, Mandl RC, Pol HEH, van den Berg LH. Motor network degeneration in amyotrophic lateral sclerosis: a structural and functional connectivity study. PLoS One 2010;5:e13664.

15. Sato K, Aoki S, Iwata NK, Masutani Y, Watadani T, Nakata Y, Yoshida M, Terao Y, Abe O, Ohtomo K, Tsuji S. Diffusion tensor tract-specific analysis of the uncinate fasciculus in patients with amyotrophic lateral sclerosis. Neuroradiology 2010;52:729–733.

16. Tsermentseli S, Leigh PN, Goldstein LH. The anatomy of cognitive impairment in amyotrophic lateral sclerosis: More than frontal lobe dysfunction. Cortex 2012;48:166-182.

17. van der Graaff MM, de Jong JM, Baas F, de Visser M. Upper motor neuron and extra-motor neuron involvement in amyotrophic lateral sclerosis: a clinical and brain imaging review. Neuromuscul Disord. 2009;19:53–58.

18. Ellis CM, Suckling J, Amaro E, Bullmore ET, Simmons A, Williams SC, Leigh PN. Volumetric analysis reveals corticospinal tract degeneration and extramotor involvement in ALS. Neurology 2001;57:1571–1578.

19. Kassubek J, Unrath A, Huppertz H-J, Lulé D, Ethofer T, Sperfeld A-D, Ludolph AC. Global brain atrophy and corticospinal tract alterations in ALS, as investigated by voxel-based

morphometry of 3-D MRI. Amyotroph. Lateral Scler. Other Motor Neuron. Disord. 2005;6:213-220.

20. Abrahams S, Goldstein LH, Suckling J, Ng V, Simmons A, Chitnis X, Atkins L, Williams SCR, Leigh PN. Frontotemporal white matter changes in amyotrophic lateral sclerosis. J. Neurol. 2005;252:321–331.

21. Cirillo M, Esposito F, Tedeschi G, Caiazzo G, Sagnelli A, Piccirillo G, Conforti R, Tortora F, Monsurrò MR, Cirillo S, Trojsi F. Widespread microstructural white matter involvement in amyotrophic lateral sclerosis: a whole-brain DTI study. AJNR Am J Neuroradiol. 2012;33:1102-1108.

22. Geser F, Brandmeir NJ, Kwong LK, Martinez-Lage M, Elman L, McCluskey L, Xie SX, Lee VM-Y, Trojanowski JQ. Evidence of multisystem disorder in whole-brain map of pathological TDP-43 in amyotrophic lateral sclerosis. Arch. Neurol. 2008;65:636–641.

23. Rose S, Pannek K, Bell C, Baumann F, Hutchinson N, Coulthard A, McCombe P, Henderson R. Direct evidence of intra- and interhemispheric corticomotor network degeneration in amyotrophic lateral sclerosis: an automated MRI structural connectivity study. NeuroImage 2012;59:2661–2669.

24. Sporns O. The human connectome: a complex network. Ann. N. Y. Acad. Sci. 2011;1224:109–125.

25. Rubinov M, Sporns O. Complex network measures of brain connectivity: uses and interpretations. NeuroImage 2010;52:1059–1069.

26. Zalesky A, Fornito A, Bullmore ET. Network-based statistic: identifying differences in brain networks. NeuroImage 2010;53:1197–1207.

27. Zalesky A, Fornito A, Seal ML, Cocchi L, Westin C-F, Bullmore ET, Egan GF, Pantelis C. Disrupted axonal fiber connectivity in schizophrenia. Biol. Psychiatry 2011;69:80–89.

28. Verstraete E, Veldink JH, Mandl RCW, Van Den Berg LH, Van Den Heuvel MP. Impaired structural motor connectome in amyotrophic lateral sclerosis. PLoS One 2011;6:e24239.

29. Verstraete E, Veldink JH, van den Berg LH, van den Heuvel M P. Structural brain network imaging shows expanding disconnection of the motor system in amyotrophic lateral sclerosis. Hum. Brain Mapp. 2014;35:1351-1361.

30. Brooks BR, Miller RG, Swash M, Munsat TL; World Federation of Neurology Research Group on Motor Neuron Diseases. El Escorial revisited: revised criteria for the diagnosis of

amyotrophic lateral sclerosis. Amyotroph. Lateral Scler. Other Motor Neuron. Disord. 2000;1:293-299.

31. Cedarbaum JM, Stambler N, Malta E, Fuller C, Hilt D, Thurmond B, Nakanishi A. The ALSFRS-R: A revised ALS functional rating scale that incorporates assessments of respiratory function. J. Neurol. Sci. 1999;169:13–21.

32. Ellis CM, Simmons A, Jones DK, Bland J, Dawson JM, Horsfield MA, Williams SC, Leigh PN. Diffusion tensor MRI assesses corticospinal tract damage in ALS. Neurology 1999;53:1051–1058.

33. Jones DK, Williams SCR, Gasston D, Horsfield MA, Simmons A, Howard R. Isotropic resolution diffusion tensor imaging with whole brain acquisition in a clinically acceptable time. Hum. Brain Mapp. 2002;15:216–230.

34. Buchanan CR, Pernet CR, Gorgolewski KJ, Storkey AJ, Bastin ME. Test-retest reliability of structural brain networks from diffusion MRI. NeuroImage 2014;86:231–243.

35. Desikan RS, Ségonne F, Fischl B, Quinn BT, Dickerson BC, Blacker D, Buckner RL, Dale AM, Maguire RP, Hyman BT, Albert MS, Killiany RJ. An automated labeling system for subdividing the human cerebral cortex on MRI scans into gyral based regions of interest. NeuroImage 2006;31:968–980.

36. Fischl B, Van Der Kouwe A, Destrieux C, Halgren E, Ségonne F, Salat DH, Busa E, Seidman LJ, Goldstein J, Kennedy D, Caviness V, Makris N, Rosen B, Dale AM. Automatically parcellating the human cerebral cortex. Cereb. Cortex 2004b;14:11–22.

37. Fischl B, Salat DH, Busa E, Albert M, Dieterich M, Haselgrove C, Kouwe AVD, Killiany R, Kennedy D, Klaveness S, Montillo A, Makris N, Rosen B, Dale AM. Whole brain segmentation: automated labeling of neuroanatomical structures in the human brain. Neuron. 2002;33:341–355.

38. Fischl B, Salat DH, Van Der Kouwe AJW, Makris N, Ségonne F, Quinn BT, Dale AM. Sequence-independent segmentation of magnetic resonance images. NeuroImage 2004a;23 Suppl. 1:S69–84.

39. Jenkinson M, Smith S. A global optimisation method for robust affine registration of brain images. Med. Image Anal. 2001;5:143–156.

40. Basser PJ, Pierpaoli C. Microstructural and physiological features of tissues elucidated by quantitative-diffusion-tensor MRI. J. Magn. Reson. B 1996;111:209–219.

41. Smith SM. Fast robust automated brain extraction. Hum. Brain Mapp. 2002;17:143–155.

42. Andersson JLR, Jenkinson M, Smith S. Non-linear registration, aka Spatial normalisation. 2007. Technical Report TR07JA2, Oxford Centre for Functional Magnetic Resonance Imaging of the Brain, University of Oxford.

43. Behrens TE, Woolrich MW, Jenkinson M, Johansen-Berg H, Nunes RG, Clare S, Matthews PM, Brady JM, Smith SM. Characterization and propagation of uncertainty in diffusion-weighted MR imaging. Magn. Reson. Med. 2003;50:1077–1088.

44. Behrens TE, Johansen-Berg H, Jbabdi S, Rushworth MFS, Woolrich MW. Probabilistic diffusion tractography with multiple fibre orientations: What can we gain? NeuroImage 2007;34:144–155.

45. Bullitt E, Gerig G, Pizer SM, Lin W, Aylward SR. Measuring tortuosity of the intracerebral vasculature from MRA images. IEEE Trans. Med. Imaging 2003;22:1163–1171.

46. Hagmann P, Cammoun L, Gigandet X, Meuli R, Honey CJ, Wedeen VJ, Sporns O. Mapping the structural core of human cerebral cortex. PLoS Biol. 2008;6:e159.

47. Van Essen DC, Ugurbil K. The future of the human connectome. NeuroImage 2012;62:1–12.

48. Funnell MG, Corballis PM, Gazzaniga MS. Cortical and subcortical interhemispheric interactions following partial and complete callosotomy. Arch. Neurol. 2000;57:185–189.

49. Embleton KV, Morris DM, Haroon HA, Lambon Ralph MA, Parker GJ. Anatomical connectivity mapping. Proc. 15th Annual Meeting of the Int. Soc. Magn. Reson. Med. (ISMRM), Berlin, Germany 2007;15:1548.

50. Smith SM, Jenkinson M, Johansen-Berg H. Tract-based spatial statistics: voxelwise analysis of multi-subject diffusion data. Neuroimage 2006;31:1487–1505.

51. Mohammadi B, Kollewe K, Samii A, Krampfl K, Dengler R, Munte TF. Changes of resting state brain networks in amyotrophic lateral sclerosis. Exp. Neurol. 2009;217:147–153.

52. Honey CJ, Thivierge JP, Sporns O. Can structure predict function in the human brain? NeuroImage 2010;52:766-776.

53. Jbabdi S, Johansen-Berg H. Tractography: where do we go from here? Brain Connect. 2011;1:169–183.

54. Zalesky A, Fornito A. A DTI-derived measure of cortico-cortical connectivity. IEEE Trans. Med. Imaging 2009;28:1023–1036.

55. Habib J, Auer DP, Morgan PS. A quantitative analysis of the benefits of cardiac gating in practical diffusion tensor imaging of the brain. Magn Reson Med. 2010;63:1098-1103.

56. Fillard P, Descoteaux M, Goh A, Gouttard S, Jeurissen B, Malcolm J, Ramirez-Manzanares A, Reisert M, Sakaie K, Tensaouti F, Yo T, Mangin J-F, Poupon C. Quantitative evaluation of 10 tractography algorithms on a realistic diffusion MR phantom. NeuroImage 2011;56:220–234.

LEGENDS

Figure 1: (a) Cortical parcellation on pial surface (healthy 56 year old male); (b) Interconnecting streamlines generated by probabilistic tractography in the same subject; (c) 85×85 connectivity matrix showing the mean weights across all subjects (N = 58), where the two large rectangular patterns on the diagonal correspond to the left and right hemispheres; (d) The histograms of network connection weights (tract-averaged FA) across all subjects in both groups.

Figure 2: Coronal, sagittal and transverse views of the impaired network nodes and interconnections identified by NBS with lobe membership indicated by color.

Figure 3: Correlations between disease progression rate and tract-averaged FA of three impaired network connections ($p < 0.05$, FDR corrected).

Figure 4: (a) Coronal, sagittal and transverse slices of the mean FA obtained from TBSS in MNI standard space, overlaid with the mean streamline density per voxel computed from the streamlines involved in the affected network and transformed to MNI space; (b) Coronal, sagittal and transverse slices of the findings from TBSS, showing the mean FA in MNI standard space overlaid with the voxels found to have significantly reduced FA in the patient group compared with the controls ($p < 0.05$, corrected).

Figure 5: Mean overlap proportion with 95% inter-percentile range (N = 58) for the 12 connections of the affected network, showing the proportion of interconnecting streamlines which pass through any white matter region identified by TBSS as having significantly reduced FA between groups.

Table 1: Global network properties (mean and standard deviation in parentheses), *t*-statistic and uncorrected *p*-value between groups.

Network measure	Patients	Controls	*t*-stat	*p*
Network sparsity	0.782 ± 0.01	0.783 ± 0.01	-0.451	0.654
Network strength	6.867 ± 0.40	6.913 ± 0.50	-0.363	0.718
Network clustering coefficient	0.227 ± 0.01	0.230 ± 0.01	-1.236	0.222
Network efficiency	0.229 ± 0.01	0.231 ± 0.01	-0.732	0.467

Table 2: Mean FA (standard deviation) and the *t*-statistic for each of the bidirectional network connections identified by NBS. All connections are collectively assigned a single *p*-value ($p = 0.020$, corrected).

Network connection	Patients	Controls	*t*-stat
Left-caudate - Left-precentral	0.37 ± 0.08	0.43 ± 0.03	3.454
Right-paracentral - Right-precentral	0.30 ± 0.04	0.33 ± 0.04	3.190
Left-paracentral - Left-superior frontal	0.29 ± 0.04	0.32 ± 0.03	3.161
Left-pallidum - Left-precentral	0.47 ± 0.04	0.50 ± 0.03	3.153
Left-superior frontal - Right-paracentral	0.44 ± 0.10	0.50 ± 0.04	3.093
Left-posterior cingulate - Right-paracentral	0.47 ± 0.04	0.50 ± 0.04	2.993
Left-superior frontal - Right-precentral	0.36 ± 0.20	0.47 ± 0.10	2.905
Left-thalamus - Left-precentral	0.45 ± 0.04	0.47 ± 0.02	2.858
Right-pallidum - Right-precentral	0.46 ± 0.04	0.48 ± 0.03	2.843
Left-caudate - Left-paracentral	0.37 ± 0.04	0.39 ± 0.03	2.783
Left-precentral - Left-superior frontal	0.36 ± 0.04	0.39 ± 0.03	2.681
Left-paracentral - Left-precentral	0.30 ± 0.04	0.33 ± 0.04	2.631

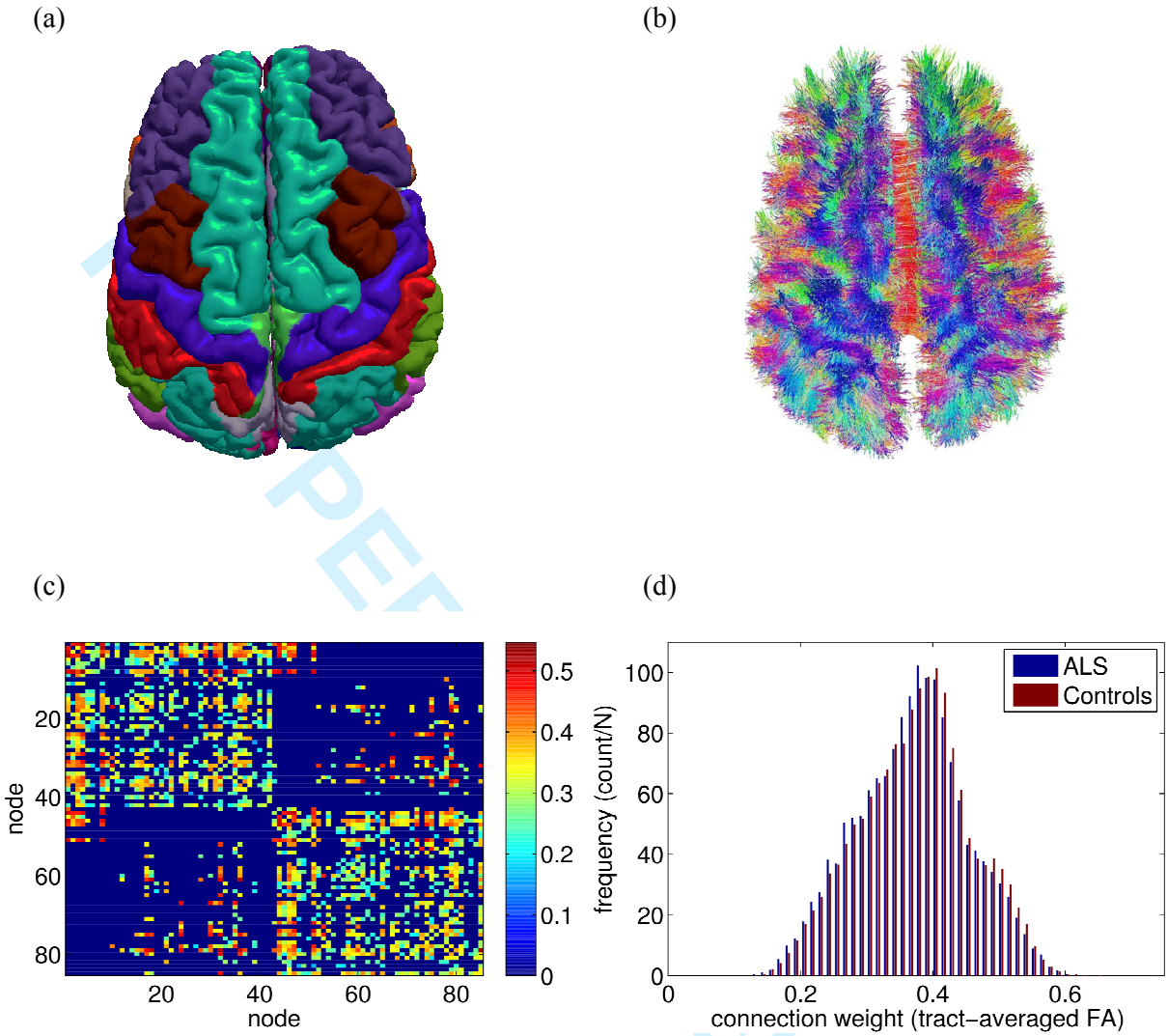
(a)
(b)
(c)
(d)
node
node
20
40
60
80
0.5
0.4
0.3
0.2
0.1
0
frequency (count/N)
connection weight (tract−averaged FA)
ALS
Controls
100
80
60
40
20
0
0.2
0.4
0.6

Figure 1

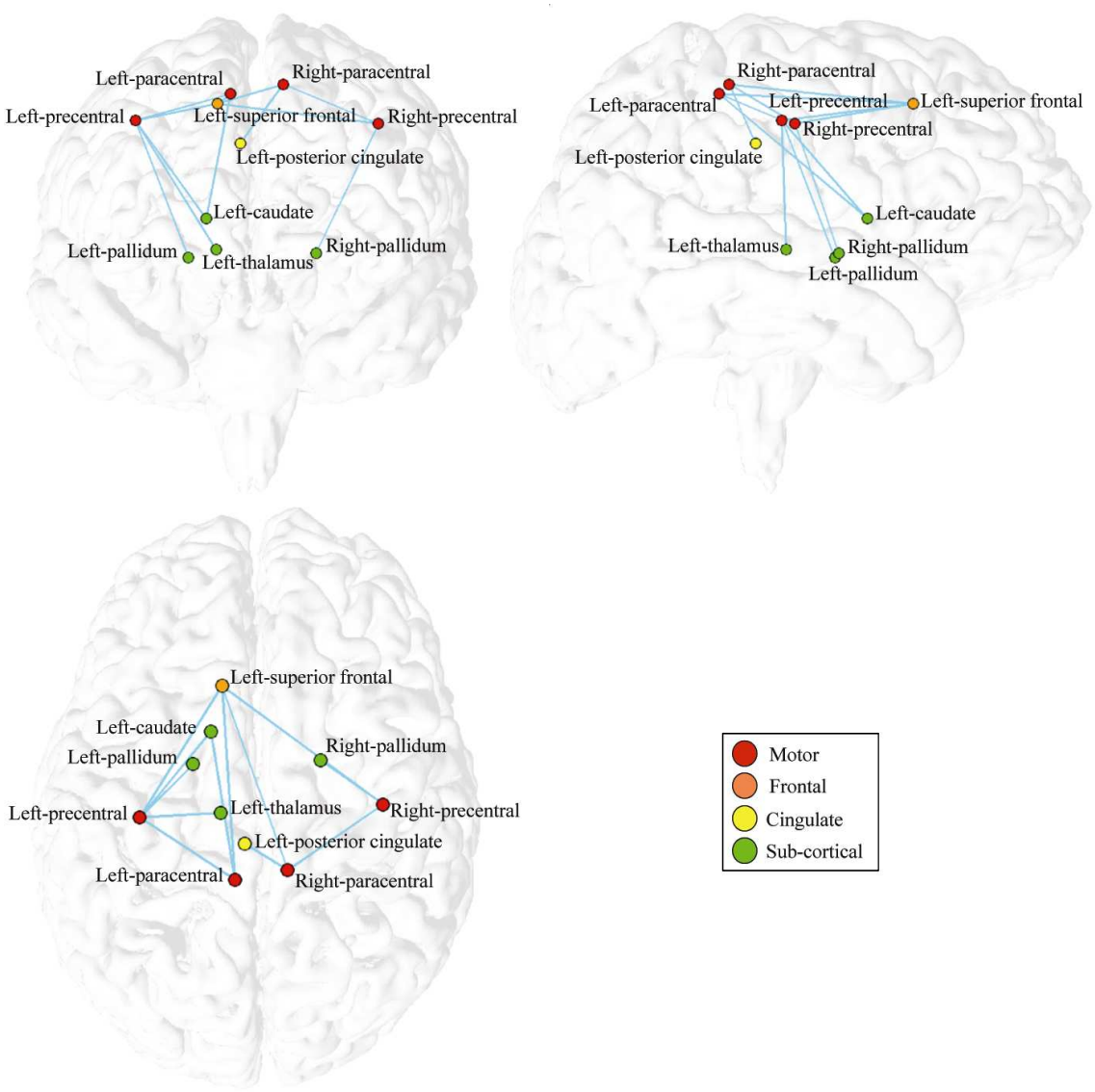

Figure 2

(a)

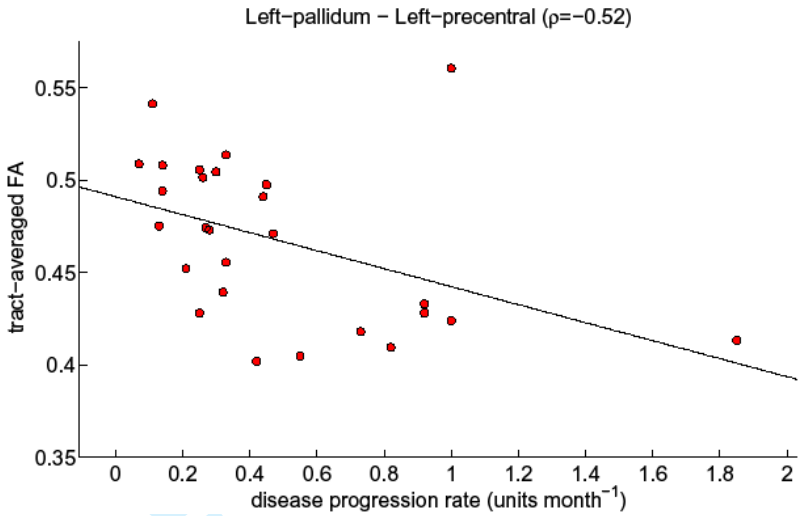
Left−pallidum − Left−precentral (ρ=−0.52)
tract−averaged FA
disease progression rate (units month^{-1})

(b)

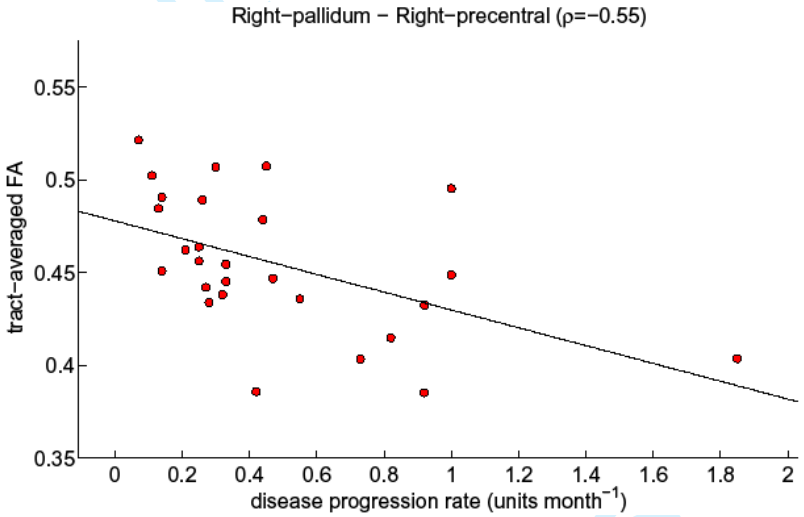
Right−pallidum − Right−precentral (ρ=−0.55)
tract−averaged FA
disease progression rate (units month^{-1})

(c)

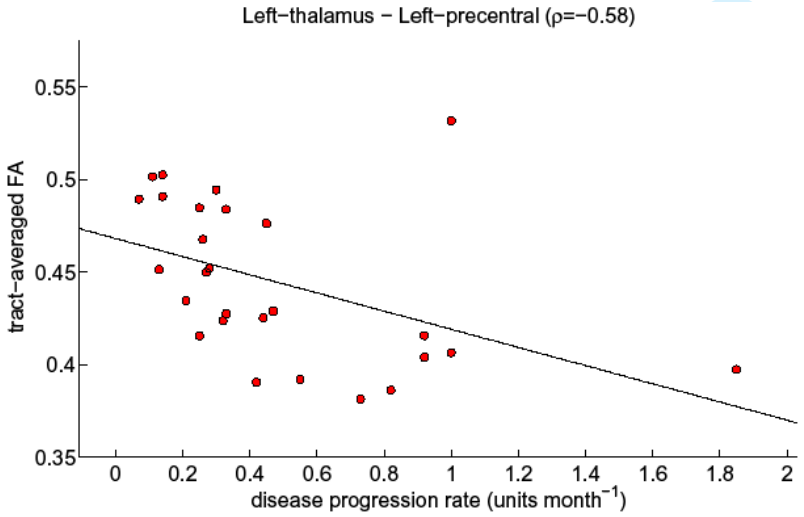
Left−thalamus − Left−precentral (ρ=−0.58)
tract−averaged FA
disease progression rate (units month^{-1})

Figure 3

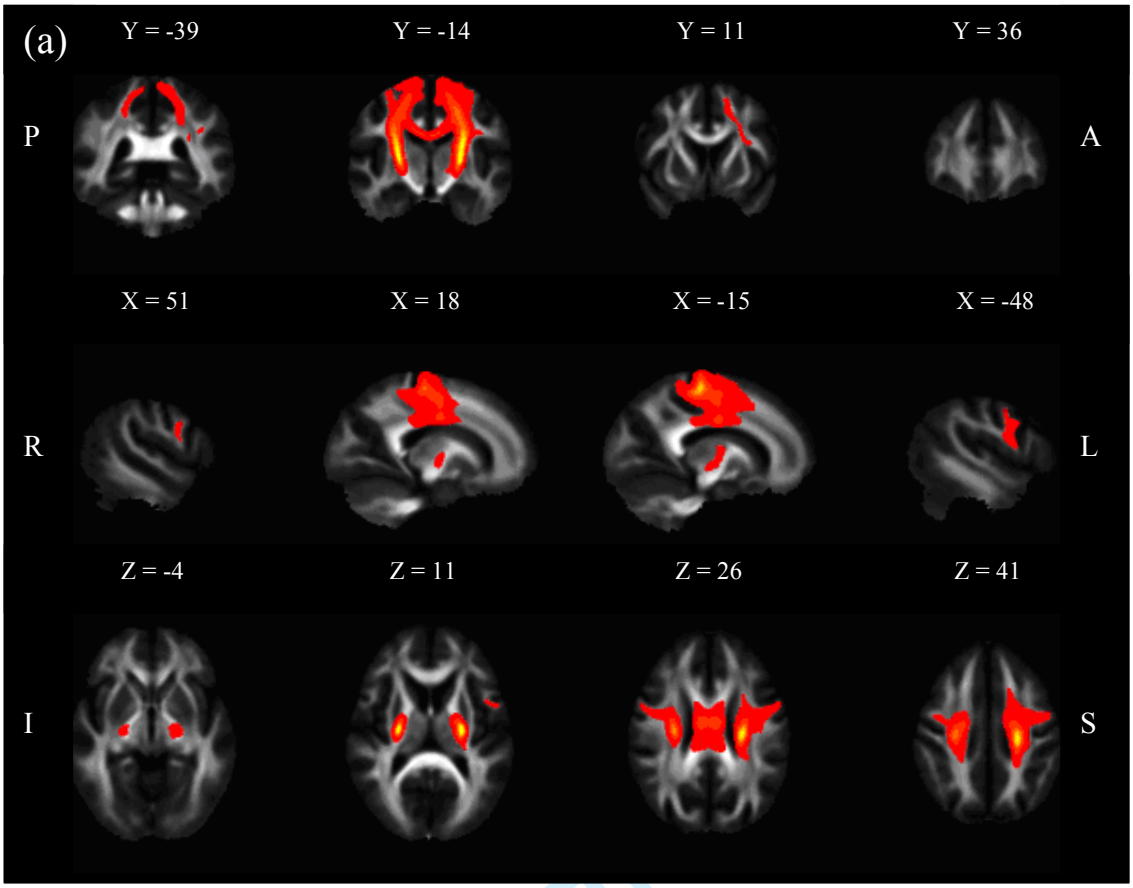

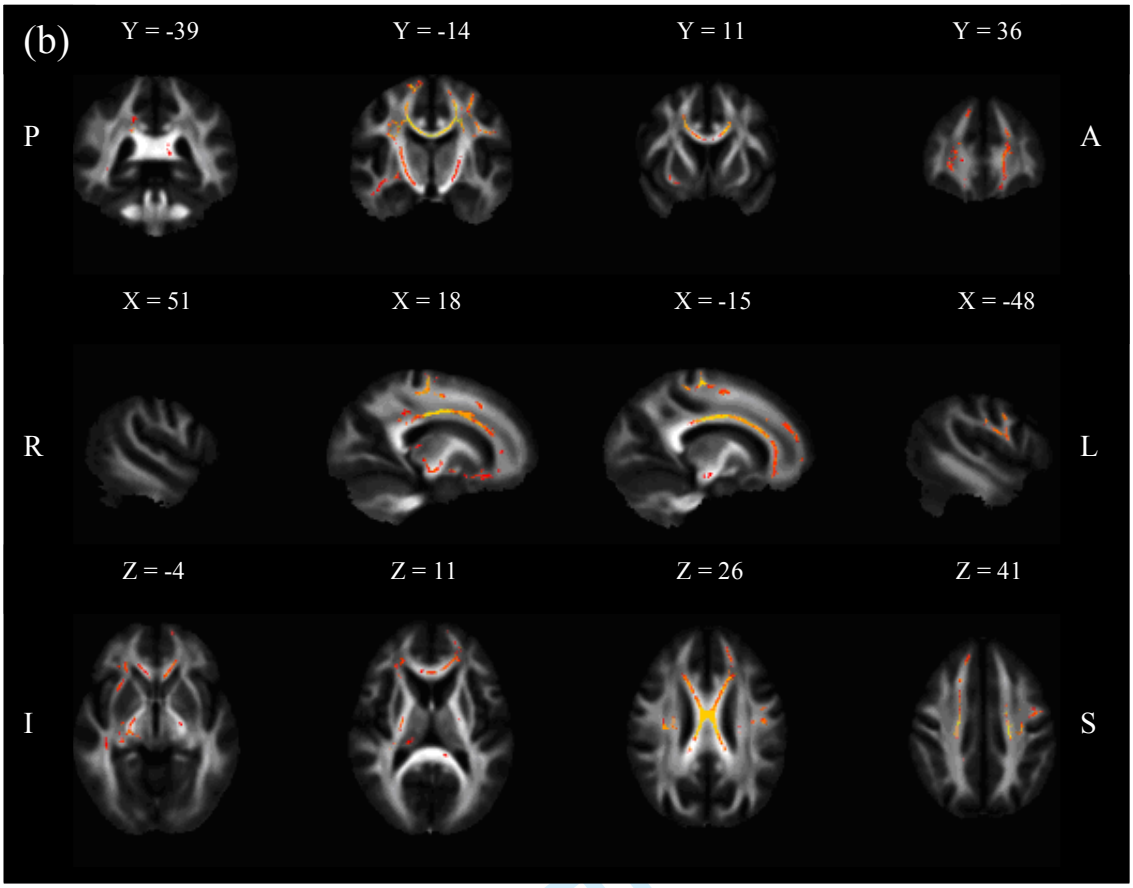

Figure 4

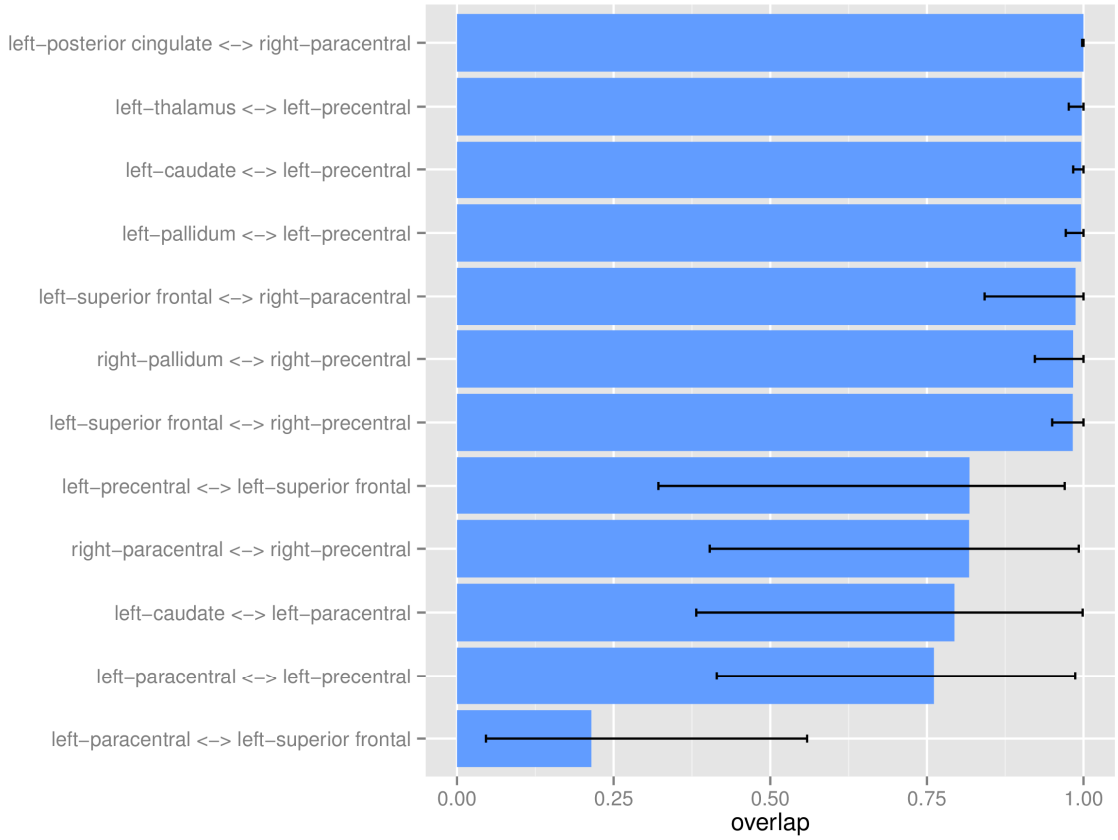

Figure 5